A Robust FACTS Damping Controller Design to Mitigate Interarea Oscillations in a Multi-machine Power System

S. M. Salehian[1] H. Hasanvand[2] B. Mozafari[3]

[1] M. Sc., Department of Electrical Engineering, Science and Research Branch, Islamic Azad University, Tehran, Iran

[2] Phd, Department of Electrical Engineering, Science and Research Branch, Islamic Azad University, Tehran, Iran
h.hasanvand@srbiau.ac.ir

[3] Phd, Department of Electrical Engineering, Science and Research Branch, Islamic Azad University, Tehran, Iran

Abstract :

In this paper, damping of interarea oscillations using simultaneous coordination of static Var compensator (SVC) and power system stabilizer (PSS) is considered. To be effective in damping of oscillations, the best-input signal of power oscillation damper (POD) associated with SVC is selected using Hankel singular values (HSVs), and right-hand plane zeros (RHP-zeros). The 4-machine-2 area standard test system, under different system configurations and loading conditions, is employed to illustrate the performance and robustness of the proposed controller. Eigenvalue analysis and nonlinear time domain simulation results demonstrate the effectiveness of the proposed technique to mitigate interarea oscillations under various operating conditions.

Keywords: Inter-area oscillations, SVC, POD, HSV, RHP-zeros.

Submission date: 31, Jan., 2015

Conditional Acceptance date:02, Oct., 2016

Acceptance date: 06, Nov., 2016

Corresponding author: H. Hasanvand

Corresponding author's address: Department of Electrical Engineering, Science and Research Branch, Islamic Azad University, Phone: +9821-44868401, P. O. Box: 775/14515, Tehran, Iran

[DOR: 20.1001.1.26765810.1396.14.4.13.0]

1. Introduction

One of the most important challenging problems in interconnected power systems is low frequency oscillations (LFOs). If adequate damping dose not provided, these oscillations can endanger system security and operation [1]. Besides PSSs, flexible ac transmission system (FACTS) devices equipped with PODs are capable of offering damping action when the system experiences LFOs. It must be noted that the damping of oscillations using FACTS devices is highly related to FACTS-based POD input signal and POD parameters [2]. Selection of POD input signal based on the different efficient techniques has been reported in the literature. Authors in [3] have used a method based on chaotic optimization algorithm for the robust coordinated design of the unified power flow controller (UPFC) power oscillation damping controller and PSS. In [4] the residue method and relative gain array (RGA) technique are used to select the best-input signal of a wide area damping controller. This hybrid method can decrease the time of signal selection process and reduce devices interaction. Application of HSVs and RHP-zeros to select the best feedback input signal of FACTS-based damping controllers is reported in [5, 6]. The RHP-zeros technique investigates various input-output combinations of transfer function zeros in both the pre-fault and post-fault conditions whereas the HSV method uses the concept of joint controllability and observability indices.

Besides signal selection process, many researchers have proposed different techniques to design the FACTS-based POD in order to improve the oscillation damping. Design of a robust H_∞ controller based on mixed sensitivity approach has been proposed to enhance of interarea oscillations damping [7]. The results show that the proposed controller is to be robust whenever change in operation point is encountered. In [8], a robust and low order-damping controller for single-input single–output system is presented. The variability of operating point is characterized by interval polynomials. Then the Kharitonov's theorem is used to design a simple damping controller. Authors in [9] have considered the simultaneous coordination of TCSC and PSS in a multi machine power system. The location of PSSs and TCSC is determined using participation factor and reside method, respectively. In addition, just the local signal is considered (as the input signal of TCSC-based POD) and residue method is used to select the input signal. A coordinated method formulated as an optimization problem which is solved using parameter-constrained nonlinear optimization algorithm. In [10], the parameters of SVC-based conventional lead-lag controller as well as membership function and scaling factors of fuzzy logic controller (FLC) are tuned optimally using improved particle swarm optimization (PSO) algorithm. The results show the effectiveness of FLC compared to lead-lag controller in damping of power oscillations in a single machine infinite bus system. A comprehensive methodology in design of centralized Takagi-Sugeno fuzzy damping controller is presented in [11]. The robustness of the proposed controller is guaranteed by satisfying specific linear matrix inequalities. Coordination of PSS and FACTS devices using evolutionary algorithms has been reported in [12, 13]. Authors in [12] have proposed the bacteria foraging optimization algorithm for the simultaneous coordinated design of PSS and SVC in a three machine-nine bus test system. The parameters of the PSS and SVC are selected in such a way that a specific cost function is minimized. A new coordinated design between PSSs and unified power flow controller (UPFC) using genetic algorithm in a 68-machine 16-bus test system has been proposed in [13].

In this paper, adopted with mentioned literature, the following modifications have been performed:

(i) Since the primary application of the SVC is to control the connected bus voltage, the best location of the SVC is selected using Q-V sensitivity as well as modal analyses. In addition, considering the suitable objective function, the size of the SVC is computed to modify the overall voltage profile of the test system.

(ii) To be effective in damping of oscillations, the best-input signal of POD is selected using HSVs and RHP-zeros analyses in both post-fault and pre-fault conditions.

(iii) Optimal tuning of SVC-POD parameters and coordination of SVC-POD and PSS is done in order to damp the oscillation modes.

The effectiveness of the proposed controller has been demonstrated using eigenvalue analysis and nonlinear time domain simulation under different contingencies. The simulations and analyses are implemented in power system analysis toolbox (PSAT) and MATLAB environments.

2. Problem formulation

2.1. Power system model

Generally, power systems can be represented by a set of non-linear differential-algebraic equations (DAE), as follows [14]:

$$\begin{aligned} \dot{x} &= f(x,y,u) \\ 0 &= g(x,y,u) \\ w &= h(x,y,u) \end{aligned} \qquad (1)$$

where x is the vector of state variables; y is the vector of algebraic variables (e.g., bus voltage magnitudes and phase angles); u is a set of controllable parameters (e.g., controller reference signals); w is a set of output variables (e.g., line current flows); f is a set of differential equations that represents system and

[DOR: 20.1001.1.26765810.1396.14.4.13.0]

controller; g is a set of algebraic equations that represents the transmission network power flows; and h is a set of equations that represents output variables (e.g., measurements), such as line power flows and rotor angle speeds. Linearizing (1) at an equilibrium point (x_0, y_0, u_0), yields:

$$\begin{bmatrix} \Delta\dot{x} \\ 0 \\ \Delta w \end{bmatrix} = \begin{bmatrix} F_x & F_y & F_u \\ G_x & G_y & G_u \\ H_x & H_y & H_u \end{bmatrix} \begin{bmatrix} \Delta x \\ \Delta y \\ \Delta u \end{bmatrix} \quad (2)$$

$$F_x = \nabla_x^T f,\ F_y = \nabla_y^T f,\ F_u = \nabla_u^T f,$$

$$G_x = \nabla_x^T g,\ G_y = \nabla_y^T g,\ G_u = \nabla_u^T g,$$

$$H_x = \nabla_x^T h,\ H_y = \nabla_y^T h,\ H_u = \nabla_u^T h$$

By eliminating the algebraic equation from system equations, the state matrix A of the system is computed as:

$$A = F_x - F_y G_y^{-1} G_x \quad (3)$$

and the state-space representation of (2) is:

$$\begin{aligned} \Delta\dot{x} &= A\Delta x + B\Delta u \\ \Delta w &= C\Delta x + D\Delta u \end{aligned} \quad (4)$$

$$B = F_u - F_y G_y^{-1} G_u$$

$$C = H_x - H_y G_y^{-1} G_x$$

$$D = H_u - H_y G_y^{-1} G_u$$

Where B and C are the input and output matrices, respectively.

In this study, a lead-lag structure for POD and PSS controllers as shown in Fig. 1 is considered. This structure includes a stabilizer gain, a washout filter, an anti-wind up limiter and two lead-lag compensator blocks. The washout block time constant (T_w) and anti-wind up limiter time constant (T_r) are set to be 10 and 0.001 s for both PSS and POD, respectively. The PSS input is speed deviation whereas the stabilization signal of PODs must be selected using the proposed method.

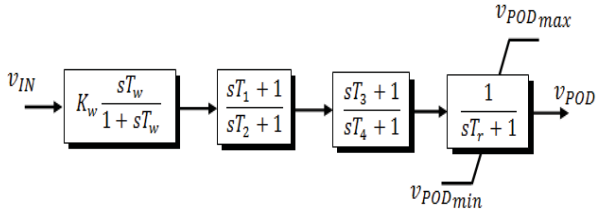

Fig 1. POD / PSS lead-lag structure.

2.1.1. POD Signal selection

Stabilizing signal for SVC-based POD is selected based on the stability indicators such as HSV and RHP-zeros. These indicators are summarized briefly in this section.

RHP-zeros: Considering the negative feedback system shown in Fig. 2 with plant $G=z/p$ and a constant gain controller $K=k$, the closed-loop transfer function is:

$$G_{cl} = \frac{KG}{1+KG} = \frac{kz}{p+kz} = k\frac{z_{cl}}{p_{cl}} \quad (5)$$

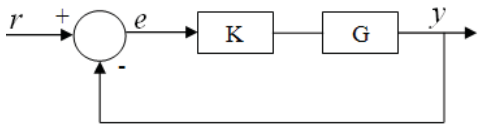

Fig. 2. Closed loop control block diagram.

where z_{cl} and p_{cl} are the closed loop zeros and poles respectively. Since different input-output can be selected, different zeros will appear. In a feedback loop system, the presence of right half plane zeros limits the potential performance of the system. When contingencies occur and the dynamic system gain increases, the closed loop poles will move toward the open loop zeros. Therefore, if these zeros are located in the right half plane of the root locus diagram, the closed loop poles could move to an unstable area and make system performance unstable. Accordingly, selection of system input-output has to be accomplished in such a way that a minimum number of zeros in the right half plane of the root locus diagram or more stable zeros with less magnitude in its real part are appeared [6].

HSVs: Observability of the input signal and controllability of the output signal are significant characteristics of POD signal selection process. The HSV technique is an interesting method to investigate the joint observability and controllability indices of each combination of inputs and outputs. The HSVs can be computed by solving following Lyapunov equations:

$$A^T Q + QA + C^T C = 0 \quad (6)$$

$$AP + PA^T + BB^T = 0 \quad (7)$$

where P and Q are controllability and observability grammian matrices, respectively. The value of the HSV can be calculated as:

$$\sigma_i = \sqrt{\lambda_i(PQ)} \quad (8)$$

where $\lambda_i(PQ)$ is the i^{th} eigenvalue of PQ. The proper POD input signal is selected based on this fact that having larger HSV will exhibit more information about system internal states and observability and controllability properties [6].

Generally, POD signal selection process can be summarized as follows:

1. All transmission lines and buses are chosen.
2. Active, reactive power and current signals of the transmission lines, bus voltages and rotor speed are considered. The lines contain local and global signals which are classified based on their type. It is worth mentioning that the signals with the same type will be analyzed by HSV criteria.
3. Signals with higher HSV magnitudes are chosen for the next step (RHP-zeros analysis).

[DOR: 20.1001.1.26765810.1396.14.4.13.0]

4. Those input signals (selected from step 3) which encounter minimum number of RHP-zeros have to be selected. This will indicate that the selected signals will have high observability and controllability properties, while making proper response to the dynamic behavior of the system.
5. When signals encountered with no RHP-zeros, the signal with more stable zeros (greater in magnitude of absolute real part) will be selected.

2.1.2. Objective function

The decaying rate of oscillations is dominated by the maximum damping factor and the amplitude of each oscillation mode is determined by its damping ratio. Thus, a proper objective function should include the damping factor and the damping ratio to design a suitable damping controller. The proposed objective function is introduced in the following:

$$Min\, F = F_1 + \varpi F_2 = \sum_{\sigma_i \geq \sigma_0} (\max_{1\leq q\leq n_q} \sigma_q - \sigma_0)^2 + \\ + \varpi \sum_{\zeta_i \geq \zeta_0} (\zeta_0 - \min_{1\leq q\leq n_q} \zeta_q)^2 \quad (9)$$

where max σ_q and min ζ_q are the maximum real part of the eigenvalues and the minimum of the damping ratio, respectively. σ_0 and ζ_0 are expected damping factor and expected damping ratio, respectively. $q=1,2,\ldots, n_q$ is the index of eigenvalues. Also, ϖ is the weight constant. The most important reason to use the objective function is this fact that besides unstable or lightly damped oscillation modes, other oscillation modes can be shifted to the left side of complex plane [15]. The constraints for both PSS and POD are expressed as follow:

$$\begin{aligned} T_{1,\min} &\leq T_1 \leq T_{1,\max} \\ T_{2,\min} &\leq T_2 \leq T_{2,\max} \\ T_{3,\min} &\leq T_3 \leq T_{3,\max} \\ T_{4,\min} &\leq T_4 \leq T_{4,\max} \\ K_{w,\min} &\leq K_w \leq K_{w,\max} \end{aligned} \quad (10)$$

3. Simulation results

The four-machine two-area test system is considered to evaluate the performance of the proposed method. Fig. 3 presents the single-line diagram of the system. In this system, each area consists of two generators .The exciter system used in each generator is a simple high gain exciter. The system loads are modeled using constant power model to consider the worst case in the design and simulation procedure. All generators have turbine-governor system whereas only second and third generators are equipped with PSS. All system data are summarized in appendix B.

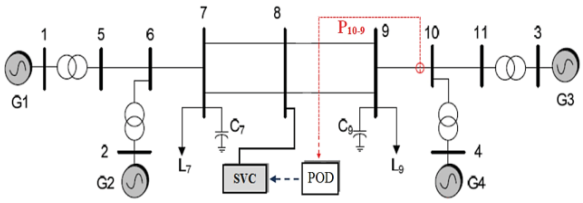

Fig. 3. The 4-machine-2 area test system.

The SVC model shown in Fig. 4 is considered as a first order block diagram. In this model, a reactance b_{SVC} is assumed and the following equation holds:

$$\dot{b}_{SVC} = (K_{SVC}(V_{ref} + V_{POD} - V) - b_{SVC})/T_{SVC} \quad (11)$$

The b_{SVC} is calculated using the following equation:

$$Q_{SVC} = -b_{SVC} V^2 \quad (12)$$

where Q_{SVC} is the reactive power injected at the SVC node.

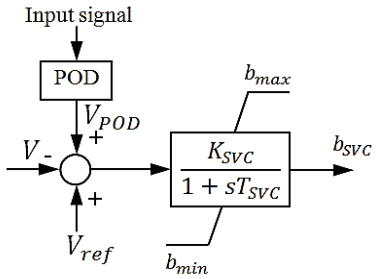

Fig. 4. Block diagram of SVC.

3.1. Placement and sizing of SVC

In order to determine the SVC location, voltage stability analysis is carried out. This technique uses the reduced power flow Jacobian matrix and performs modal calculations to determine the weakest bus that needs reactive power compensation. Bus #8 has the greatest sensitivity to voltage and reactive power variations and hence this bus is potential candidate to install SVC. Mvar sizing of SVC plays an important role in analyzing the system dynamic response. For a level of load the following objective function is to be minimized [6]:

$$\sum_{i=1}^{No.Bus} \left|(V_i - 1)^3\right| \quad (13)$$

Using this objective function yields the optimal Mvar size SVC in such a way that the overall bus voltages become approximately close to 1 pu. The obtained results by PSO algorithm show that a 150-Mvar SVC has to be placed in the system at bus 8 for voltage stability. The voltage profile before and after compensation has been depicted in Fig. 5.

[DOR: 20.1001.1.26765810.1396.14.4.13.0]

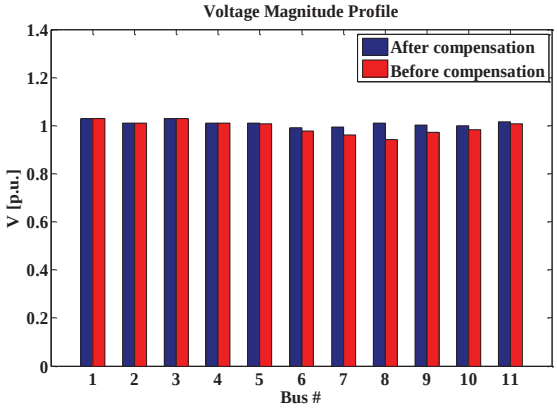

Fig. 5. Voltage magnitude profile before and after compensation.

3.2. Signal selection

The active, reactive power and current of transmission lines, bus voltages and speed of generators are taken into account as input signals to POD. These signals are listed in the following:

$P_{5\text{-}6}$, $P_{6\text{-}7}$, $P_{8\text{-}9}$, $P_{7\text{-}8}$, $P_{10\text{-}11}$, $P_{9\text{-}10}$, $Q_{5\text{-}6}$, $Q_{6\text{-}7}$, $Q_{8\text{-}9}$, $Q_{7\text{-}8}$, $Q_{10\text{-}11}$, $Q_{9\text{-}10}$, $I_{5\text{-}6}$, $I_{6\text{-}7}$, $I_{8\text{-}9}$, $I_{7\text{-}8}$, $I_{10\text{-}11}$, $I_{9\text{-}10}$, V_5, V_6. V_7, V_9, V_{10}, V_{11}, w_1, w_2, w_3, w_4.

The HSV diagrams of mentioned signals for pre-fault and post-fault are shown in Figs. 6-10. The signals with higher magnitudes in each type are selected to be analyzed by RHP-zeros criteria. The signals associated with higher HSVs in each category are summarized in Table 1. These signals are all considered to investigate the RHP-zeros criteria of the open loop transfer functions for both pre-fault and post-fault conditions (see Table 1). It is clear from Table 1 that only $P_{10\text{-}9}$ and $P_{6\text{-}7}$ have not produced any RHP-zeros, hence a more detailed investigation should be done to choose the best signal. The zero diagrams of open loop transfer functions related to $P_{10\text{-}9}$ and $P_{6\text{-}7}$ and SVC output in pre-fault and post-fault conditions have been depicted in Fig. 11. It is clear from Fig. 11 that $P_{10\text{-}9}$ produced more stable open loop zeros that have higher real amplitude compared to $P_{6\text{-}7}$. Therefore, the selected input signal for POD is $P_{10\text{-}9}$.

3.3. Optimal tuning of POD parameters

In this section, simultaneous coordination of PSS and SVC-POD parameters is carried out by minimizing the objective optimization problem given in (9). In order to obtain the suitable results, PSO code is run for 10 times separately with different random populations. The PSO parameters are: population size=50, itermax=100, learning coefficients =2. The expected damping factor and damping ratio are selected as: $\sigma_0 = -2$ and $\zeta_0 = 0.4$, respectively. The value of ϖ as a weighting coefficient is selected to be 10, which is derived from the experiences of many experiments conducted on this problem. The upper and lower limits of variables are summarized in Table 2. In this paper, to show the robustness of the proposed controllers, four operating conditions are considered as follow:

Case 0: Nominal loading condition, a three phase fault at bus 7 at 0.1 sec and removed after 90 ms and the breaker operates to disconnect one of tie-lines between bus 7 and bus 8.

Case 1: Nomonal loading condition, A three phase fault at bus 9 at 0.1 sec and removed after 90 msec.

Case 2: Nomonal loading condition, outage of tie line 8-9 at t=1sec.

Case 3: Heavy loading condition (140% of its rated load), a three phase fault at bus 7 at 0.1 sec and removed after 90 ms and the breaker operates to disconnect one of tie-lines between bus 7 and bus 8.

Table 1. RHP-zeros analysis of the selected signals from HSV analyzing part.

Selected signals for RHP-zeros	Pre-fault	Post-fault
	RHP-zeros	RHP-zeros
$P_{9\text{-}10}$	**No**	**No**
$P_{6\text{-}7}$	No	No
$Q_{9\text{-}10}$	Yes	Yes
$Q_{6\text{-}7}$	Yes	Yes
$I_{9\text{-}10}$	Yes	Yes
$I_{6\text{-}7}$	Yes	Yes
V_7	Yes	Yes
V_9	Yes	Yes
w_{G1}	Yes	Yes
w_{G2}	Yes	Yes

Table 2. Upper and lower limits of parameters.

Case		Lower Limit	Upper Limit
PSS	K	0.001	100
	T_i (i=1,2,3,4)	0	2
POD controller	K	0.001	100
	T_i (i=1,2,3,4)	0	2

The tuning techniques are carried out for case 0 and the resulting parameters are kept constant for other cases to show the robustness of the proposed controllers. Optimal parameters of POD as well as coordinated parameters of POD and PSSs are tabulated in Table 3. Table 4 shows the eigenvalues and related damping ratio of electromechanical oscillation modes. As can be seen from this table, the damping ratio of the interarea oscillation mode is improved satisfactorily using the POD, but there is no remarkable change in damping of local modes. In addition, using the coordinated POD and PSSs, besides the interarea mode, the local modes are also relocated, and their damping ratio is improved significantly. The eigenvalues are depicted in Figs. 12-13. The results reveal that the proposed coordinated controller not only relocate the interarea oscillation

[DOR: 20.1001.1.26765810.1396.14.4.13.0]

mode but shifts local oscillation modes to the more stable area in the s-plane.

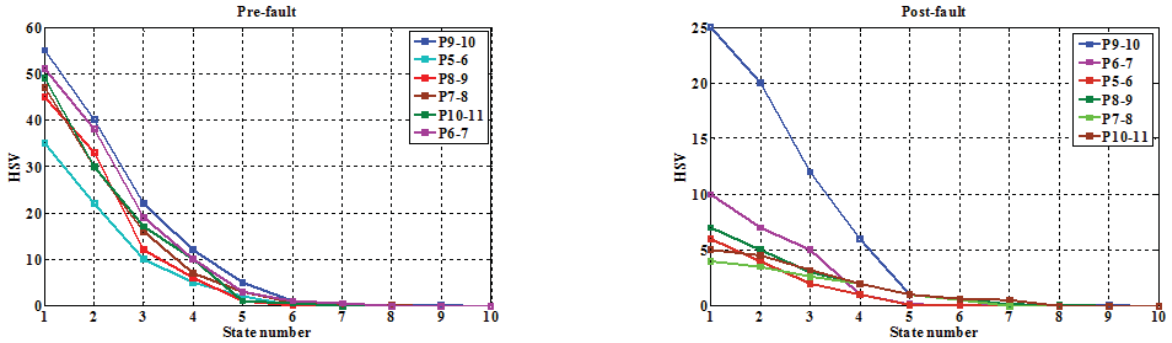

Fig. 6. HSV diagrams for active power signals.

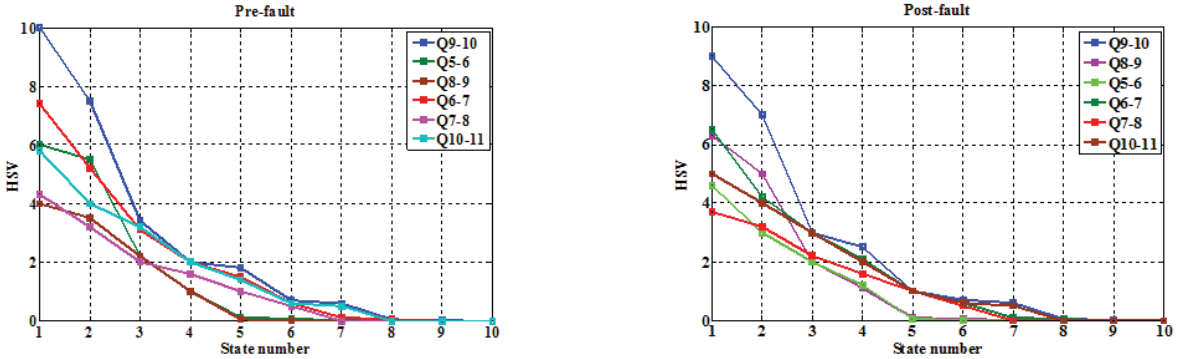

Fig. 7. HSV diagrams for reactive power signals.

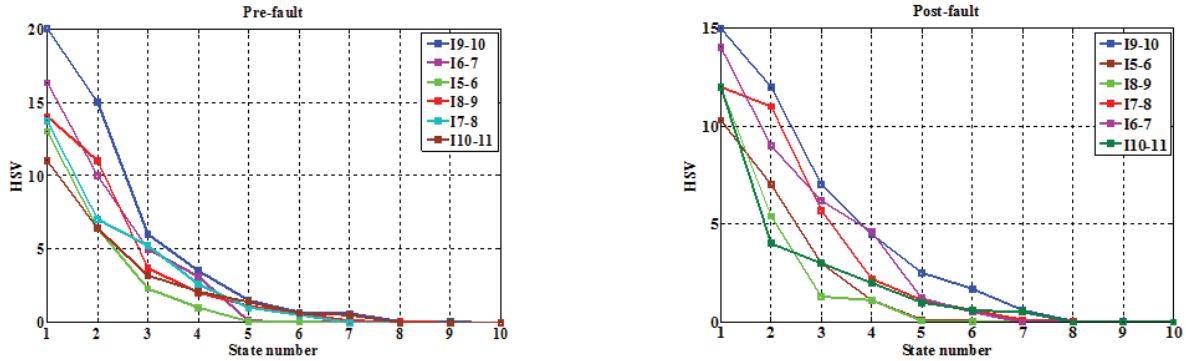

Fig. 8. HSV diagrams for line current signals.

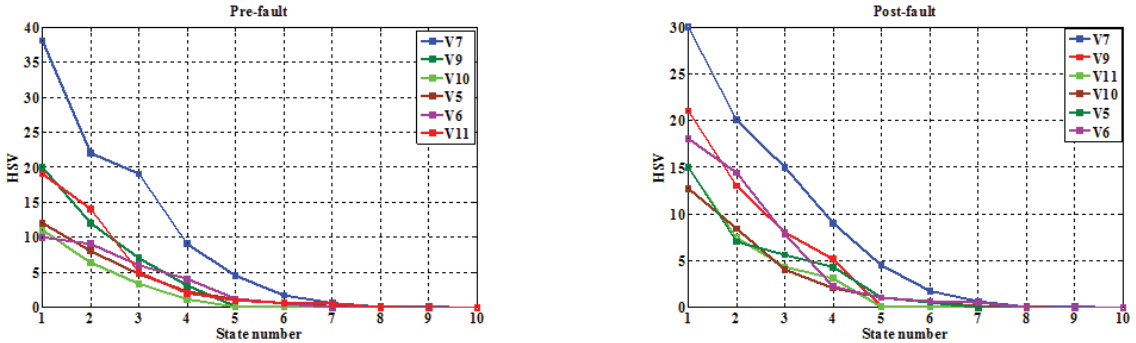

Fig. 9. HSV diagrams for bus voltage signals.

[DOR: 20.1001.1.26765810.1396.14.4.13.0]

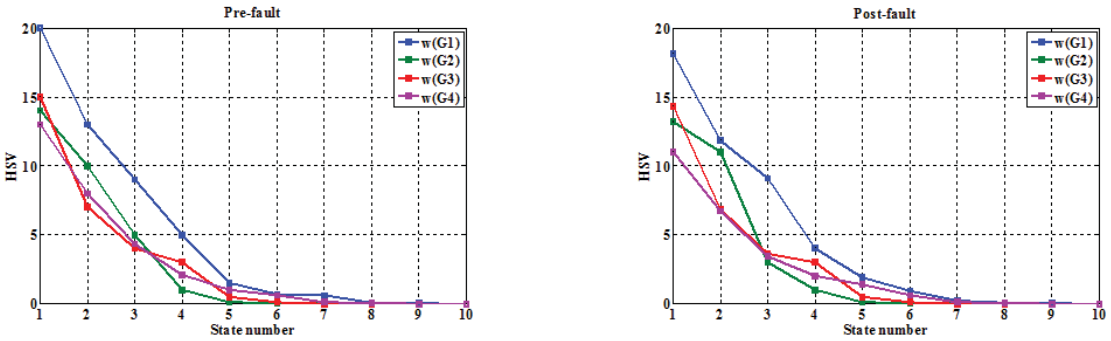

Fig. 10. HSV diagrams for generator speed signals.

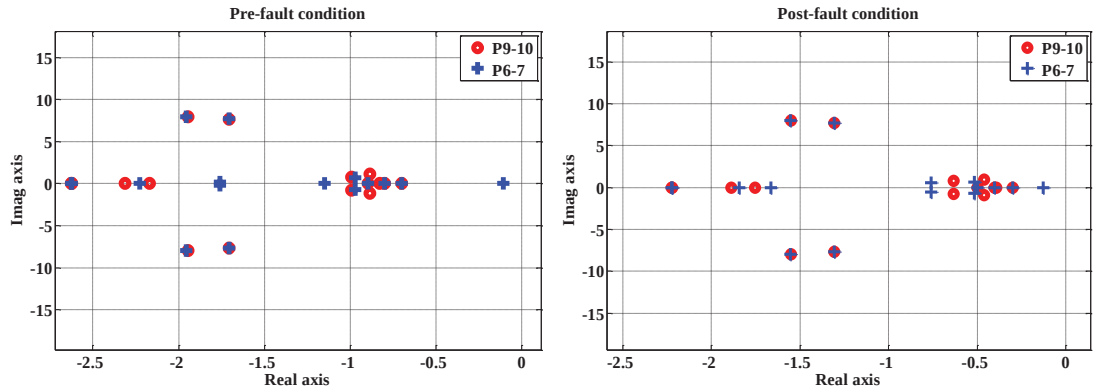

Fig. 11. Zero plots of transfer functions related to SVC output and $P_{10\text{-}9}$ and $P_{6\text{-}7}$.

Table
4 shows the eigenvalues and related damping ratio of electromechanical oscillation modes

Table 3. Optimal control parameters

Only POD	K	T_1	T_2	T_3	T_4
Optimal POD	9.8	.001	1.875	.001	.202
Coordination of POD & PSS	K	T_1	T_2	T_3	T_4
Optimal POD	10.15	.001	0.953	1.1962	1.4803
Optimal G2-PSS parameters	24.126	.5878	.0778	.4738	.9828
Optimal G3-PSS parameters	11.4872	1.0953	.247	1.358	1.5394

A number of time domain simulations are performed to demonstrate the effectiveness of the proposed controllers. Figs. 14–21 show the speed deviation response of G1-G2 (representative of local mode) and G1-G3 (representative of interarea mode) for mentioned cases [17]. These results show the effectiveness of the proposed controllers to damp out electromechanical oscillation modes. As can be seen from Figs. 14-21, the designed controllers are robust in damping of oscillations under system operating condition variations. In addition, the results reveal that the coordinated design of the POD and PSSs can damp out electromechanical oscillations in terms of local and interarea modes more effectively when compared to PSS.

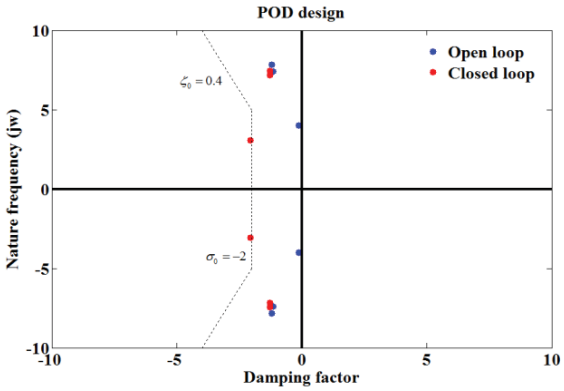

Fig. 12. Open and closed loop eigenvalues (only POD).

[DOR: 20.1001.1.26765810.1396.14.4.13.0]

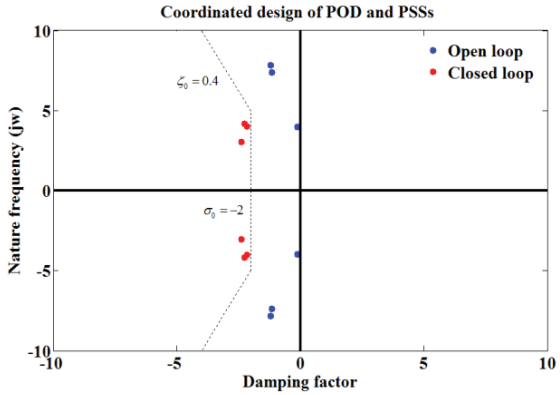

Fig. 13. Open and closed loop eigenvalues (coordinated design of POD and PSSs).

Table 4. Electromechanical oscillation modes.

Case	Modes	Eigenvalues	Damping ratio	Frequency (Hz)
SVC	Local1	-1.184±j7.8201	0.149	1.258
	Local2	-1.157±j7.3945	0.154	1.191
	Interarea	-0.111±j3.9908	0.027	0.635
With POD	Local1	-1.2732 ±j7.435	0.168	1.18
	Local2	-1.2663 ±j7.183	0.173	1.14
	Interarea	**-2.0584 ±j3.058**	0.558	0.48
Coordination of POD & PSS	**Local1**	**-2.2632 ±j4.175**	**0.476**	**0.664**
	Local2	**-2.1567 ±j4.023**	**0.472**	**0.640**
	Interarea	**-2.3699 ±j3.033**	**0.615**	**0.483**

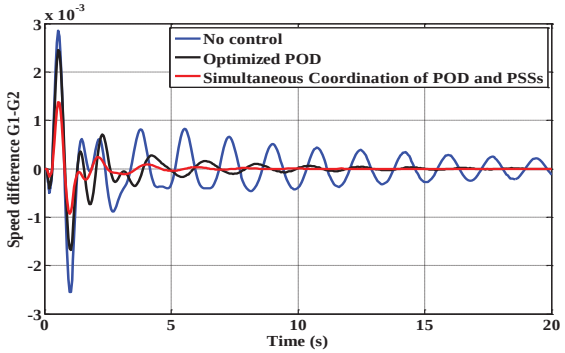

Fig. 14. Speed difference response of G1-G2 for case 0.

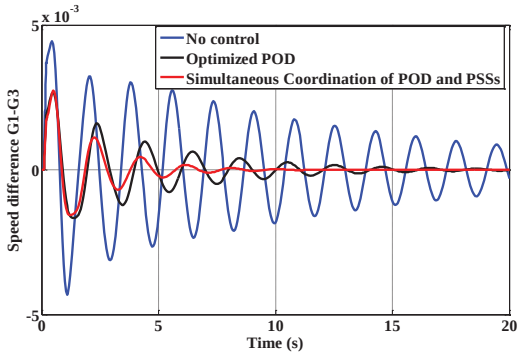

Fig. 15. Speed difference response of G1-G3 for case 0.

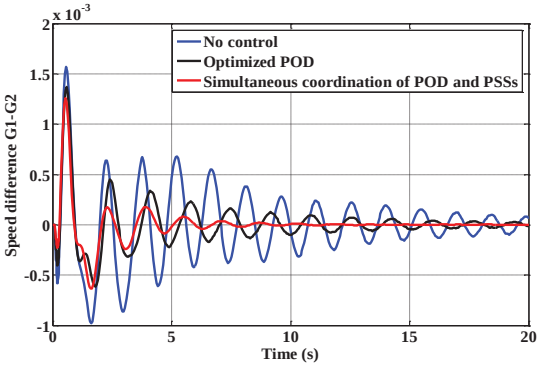

Fig. 16. Speed difference response of G1-G2 for case 1.

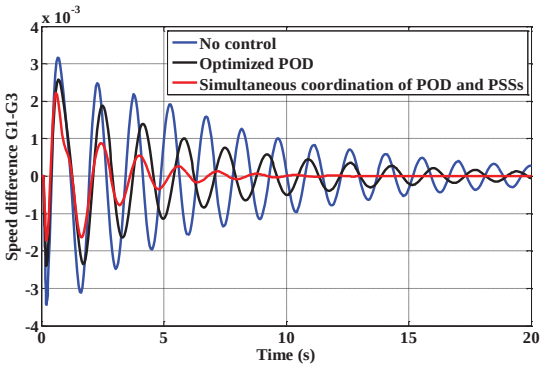

Fig. 17. Speed difference response of G1-G3 for case 1.

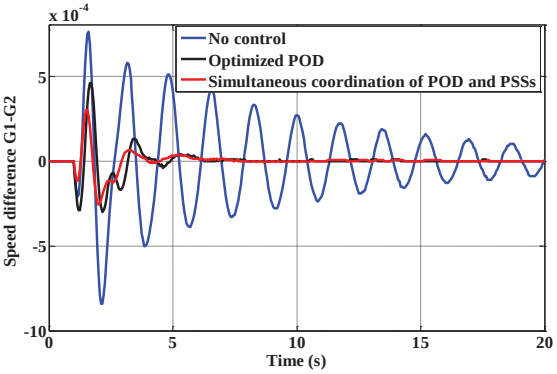

Fig. 18. Speed difference response of G1-G2 for case 2.

[DOR: 20.1001.1.26765810.1396.14.4.13.0]

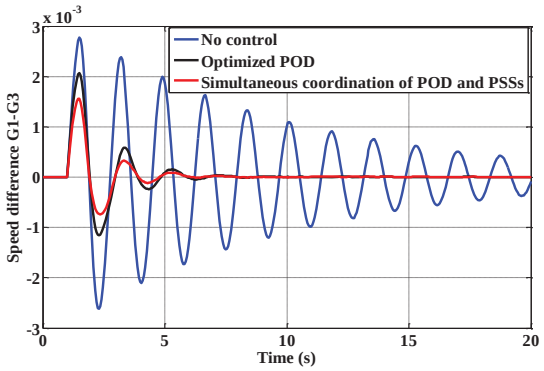

Fig. 19. Speed difference response of G1-G3 for case 2.

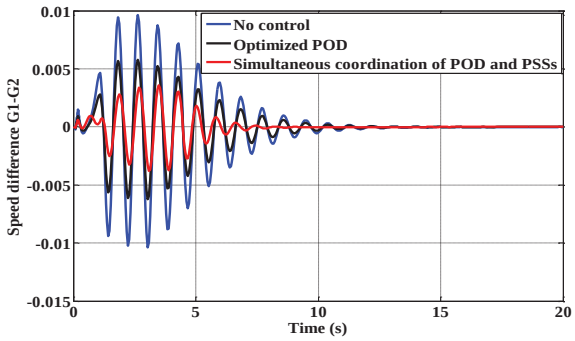

Fig. 20. Speed difference response of G1-G2 for case 3.

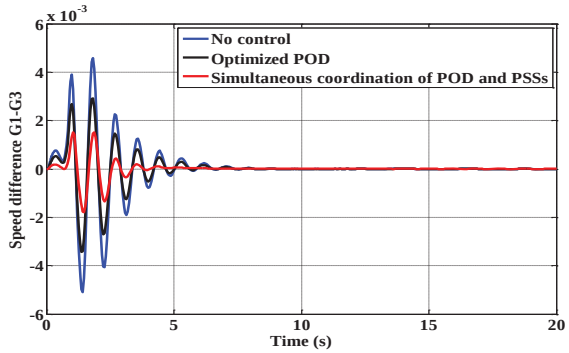

Fig. 21. Speed difference response of G1-G3 for case 3.

4. Conclusion

The main purpose of this paper is to design the SVC-POD to damp-out low frequency power oscillations besides maintaining SVC primary function that is the improvement of voltage stability. Therefore, the location of FACTS devices is determined based on static voltage stability. Also, PSO algorithm is used to find the optimal size of SVC. Then, the input signal to the PODs is determined using HSVs and RHP-zeros analyses. In addition, optimal values of control parameters of the PODs are computed considering the novel objective function solving by the PSO algorithm. Finally, simultaneous coordination of POD and PSSs has been implemented. The results show that the proposed controller is effective in damping of low frequency oscillations while the primary application of SVC in terms of improving voltage stability and increasing loading factors is guaranteed.

Appendix

1. PSO Algorithm Parameters

The PSO parameters are summarized as Population size: 50, Maximum iteration: 100, c1= c2= 2. The computations were performed by an Intel (R) Core™ 2 duo. The processor having a speed of 2.66 GHz and an installed memory (RAM) of 3.00 GB. The CPU time in calculation of optimal parameters of POD as well as coordinated POD and PSS is 2453 and 2868 second respectively.

2. Two-area-four-machine test system data [1]

Generators data:

$$R_a = 0.0025; x_d = 1.8; x_l = 0.2; x'_d = 0.3$$
$$x''_d = 0.25; \tau'_{do} = 8s; \tau''_{do} = 0.3s; x_q = 1.7$$
$$x'_q = 0.55; x''_q = 0.25$$
$$\tau'_{qo} = 0.4s; \tau''_{qo} = 0.5s; H_{G1} = H_{G2} = 5.5$$
$$H_{G3} = H_{G4} = 5$$

SVC data:

T_{SVC}= 0.05s; K_{SVC}=50; b_{max}=2pu; b_{min}= -1pu; V=230; V_{ref} =1.011 pu.

Governor data:

Servo time constant Ts = 0.1s; Governor Time constant= 0.5s; Transient gain time constant T_3= 0s; HP section time constant T_4= 1.25s; Re-heater time constant T_5=5s.

Exciter data:

Voltage regulator gain K_A=200; Voltage regulator time constant T_A=0s; $V_{R\text{-}max}$=10; $V_{R\text{-}min}$= -10.

Transmission line data:

Nominal voltage, 230 kV; S_{base}=100MVA; r=0.0001 pu/km; x_L=0.001 pu/km, b_c=0.00175 pu/km.

The overall system data can be found in [1].

References

[1] P. Kundur, Power system stability and control, McGraw-Hill, New York, 1994.

[2] N. Magaji, and M. W. Mustafa, "Optimal location and signal selection of UPFC device for damping oscillation", Int Journal of Elec. Power and Energy Syst., vol. 33, pp. 1031–1042, 2011.

[3] A. Safari, H. Shayeghi and S. Jalilzadeh, " Robust Coordinated Design of UPFC Damping Controller and PSS Using Chaotic Optimization Algorithm", Journal of Iranian Association of Electrical and Electronics Engineers., vol. 12, no. 3, Winter 2015.

[4] N. Yang, Q. Liu and J. D. Calle, "TCSC Controller Design for Damping Interarea Oscillations", IEEE Trans. Power Syst., vol. 13, pp. 1304-1310, 1998.

[5] Y. Li, C. Rehtanz, S. Rüberg, L. Luo and Y. Cao, "Assessment and Choice of Input Signals for Multiple HVDC and FACTS Wide-Area Damping Controllers", IEEE Trans. Power Syst., vol. 27, pp. 1969-1977, 2012.

[6] M. Farsangi, H. Nezamabadi-pour, S. Yong-Huna and K. Y. Lee, "Choice of FACTS Device Control Inputs for Damping Inter-area Oscillations", IEEE Trans. Power Syst., vol. 19, pp. 1135-1143, 2004.
[7] M. Farsangi, H. Nezamabadi-pour, S. Yong-Huna and K. Y. Lee, "Placement of SVCs and Selection of Stabilizing Signals in Power Systems", IEEE Trans. Power Syst., vol. 22, pp. 1061-1071, 2007.
[8] B. Chaudhuri, B. C. Pal, A. C. Zolotas, I. M. Jaimoukha and T. C. Green, "Mixed-Sensitivity Approach to H∞ Control of Power System Oscillations Employing Multiple FACTS Devices", IEEE Trans. Power Syst., vol. 18, pp. 1149-1156, 2003.
[9] D. D. Simfukwe, and B. C. Pal, "Robust and Low Order Power Oscillation Damper Design Through Polynomial Control", IEEE Trans. Power Syst., vol. 28, pp. 1599-1608, 2013.
[10] L. J. Cai, and I. Erlich, "Simultaneous Coordinated Tuning of PSS and FACTS Damping Controllers in Large Power Systems", IEEE Trans. Power Syst., vol. 20, pp. 294-300, 2005.
[11] H. Hasanvand, B. Bakhshideh Zad, B. Mozafari and B. Feizifar, "Damping of Low-Frequency Oscillations using an SVC-Based Supplementary Controller", IEEJ Trans., vol. 8, pp. 550–556, 2013.
[12] B. P., Padhy, S. C. Srivastava and N. K. Verma, "Robust Wide-Area TS Fuzzy Output Feedback Controller for Enhancement of Stability in Multimachine Power System", IEEE Syst Journal., vol. 6, pp. 426-436, 2012.
[13] S. M. Abd-Elazim, and E. S. Ali, "Coordinated design of PSSs and SVC via bacteria foraging optimization algorithm in a multimachine power system", Int Journal of Elect. Power and Energy Syst., vol. 41, pp. 44–53, 2012.
[14] L. H. Hassan, M. Moghavvemi, H. A. F. Almurib and K. M. Muttaqi, A Coordinated Design of PSSs and UPFC-based Stabilizer Using Genetic Algorithm, IEEE Transactions on Industry Applications., vol. 50, pp. 1-9, 2014.
[15] H. M. Ayres, I. Kopcak, M. S. Castro, F. Milano, V.F. da Costa, "A didactic procedure for designing power oscillation dampers of FACTS devices", Simulation Modeling Practice and Theory., vol. 18, pp. 896-909, 2010.
[16] S. K. Wang, J. P. Chiou and C. W. Liu, "Parameters tuning of power system stabilizers using improved ant direction hybrid differential evolution", Int Journal of Elect. Power and Energy Syst., vol. 31, pp. 34–42, 2009.

[DOR: 20.1001.1.26765810.1396.14.4.13.0]